

Electronic Supplementary Information for

Supramolecular multicompartment gels formed by ABC graft copolymers: high toughness and recovery properties

Pengxiang Xu, Jiaping Lin, and Liangshun Zhang**

Shanghai Key Laboratory of Advanced Polymeric Materials, State Key Laboratory of Bioreactor Engineering, Key Laboratory for Ultrafine Materials of Ministry of Education, School of Materials Science and Engineering, East China University of Science and Technology, Shanghai 200237, China

E-mail: jlin@ecust.edu.cn (J. Lin), zhangls@ecust.edu.cn (L. Zhang)

1. Equilibrium structures of ABC graft copolymer solutions and gels

Figure S1 shows the structural snapshots of ABC graft copolymers with and without hydrogen bonding groups in solutions under various polymer concentrations ϕ . The molecular architectures in all the systems are identical, *i.e.*, the backbone and each graft chain respectively contain 51 and 3 beads, and the position of the first graft point s_1 is fixed at 0.02. It can be seen that the structures in the systems with and without hydrogen bonding interactions are similar at the same ϕ . The ABC copolymers at $\phi = 0.10$ and 0.40 form isolated micelles (Figure S1a, c) and multicompartment gels (Figure S1b, d), respectively. It should be pointed out that the solvophobic **B** and **C** grafts in the multicompartment gels are segregated into different domains, which are connected by the solvophilic **A** backbones.

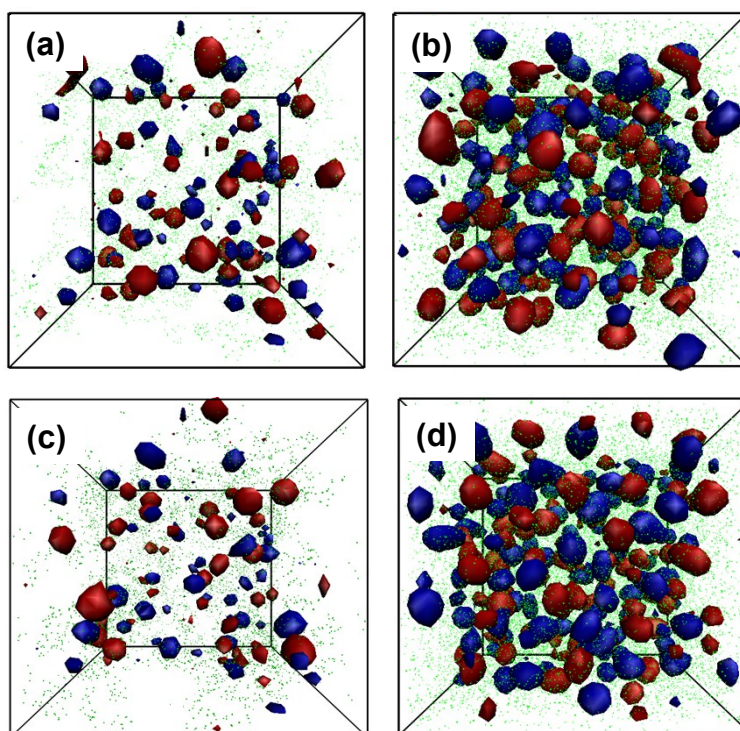


Figure S1. Structural snapshots of ABC graft copolymers containing hydrogen bonding groups in solutions with (a) $\phi = 0.10$ and (b) $\phi = 0.40$. Structural snapshots of ABC copolymers without hydrogen bonding groups in solutions with (c) $\phi = 0.10$ and (d) $\phi = 0.40$. The green particles are the **A** beads, and the blue (red) colors are assigned to the **B**-rich (**C**-rich) domains.

2. Orientation behavior of graft chains

The orientation behavior of graft chains is examined. The orientation degree $\langle p_g \rangle$ of grafts is given by $(3\langle \cos \theta_g \rangle - 1)/2$, where θ_g is the angle between the tensile direction and the end-to-end vector of grafts (see the inset of Figure S2). Figure S2 shows the $\langle p_g \rangle$ as a function of strain for ABC copolymer solutions with various ϕ . Similar to the evolution of average bond length $\langle l_b \rangle$ and bond orientation parameter $\langle p_2 \rangle$, the value of $\langle p_g \rangle$ gradually increases in the elongation process, further indicating that the grafts are gradually orientated along the tensile direction.

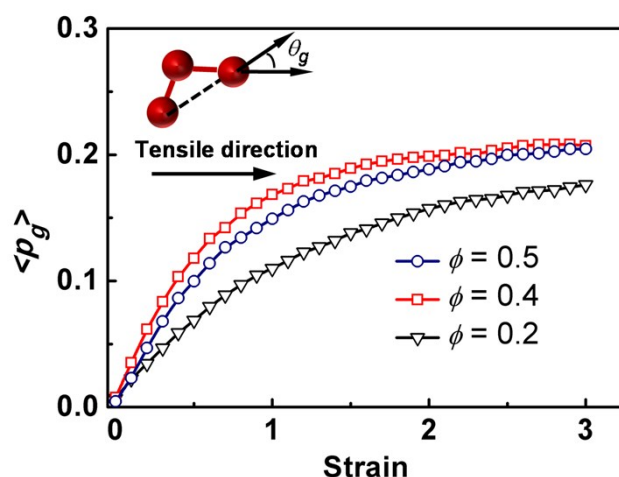


Figure S2. $\langle p_g \rangle$ as a function of strain for ABC copolymer solutions with various ϕ . The inset shows the definition of angle θ_g between the tensile direction and the end-to-end vector of the grafts.

3. Affine and non-affine deformation of the gels

The affine and non-affine deformations of the gels were examined by tracking the positions of tracer beads in the elongation process. Figure S3a shows the x -component r_x of the position vector of six tracer beads which are randomly picked. It can be viewed that the beads with the same r_x at initial state (such as the 120-*th* and 356-*th* beads) have different r_x values with increasing strain.

This implies that the deformation is not uniform and non-affine deformation takes place. We then examined the non-affine deviation, u , which is defined as the distance between the real position and the affine position. The mean squared non-affine deformation $\langle u^2 \rangle$ for the polymer beads and polymer chains were calculated and normalized by the affine deformation. Figure S3b shows the relation between the $\langle u^2 \rangle$ and the strain. It can be viewed the $\langle u^2 \rangle$ for the polymer beads is slightly larger than that for polymer chains. More importantly, the non-affine deformation is small compared to the affine deformation at smaller strain, and thus the stress-strain relationship is linear in this regime. As the strain increases, the non-affine deformation becomes comparable to the affine deformation, leading to the non-linear stress-strain relationships at larger strain

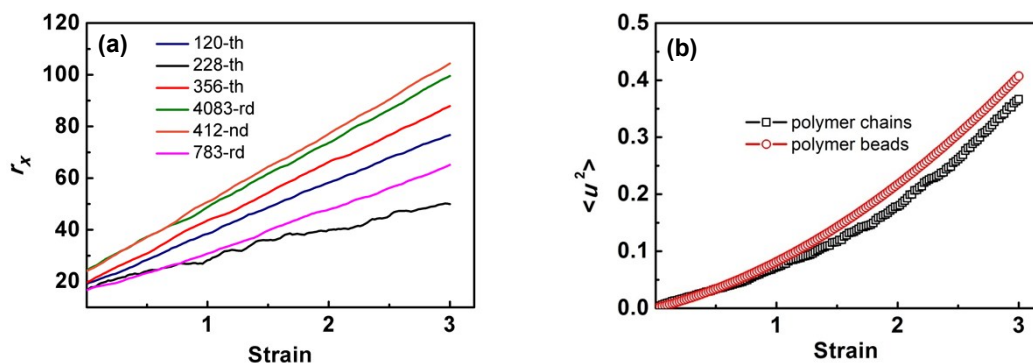


Figure S3. (a) Position of representative polymer beads and (b) non-affine deformation as a function of strain for ABC copolymer gel under tension with strain rate of $0.2\tau^{-1}$. The polymer concentration is $\phi=0.40$.

4. Rigorous solutions of the rate equations

In the elongation process, the donor D -beads and the acceptor A -beads of hydrogen bonds in the C grafts can form the associated bodies $A\cdot D$. Meanwhile, the $A\cdot D$ is able to disassociate into A and D . The concentrations of A , D , and $A\cdot D$ satisfy the rate equations

$$\frac{d[A]_t}{dt} = -k_a[A]_t[D]_t + k_d[A \cdot D]_t \quad (S1)$$

$$\frac{d[A \cdot D]_t}{dt} = k_a[A]_t[D]_t - k_d[A \cdot D]_t \quad (S2)$$

where k_a and k_d are the association and disassociation rates, respectively. The $[A]_t$, $[D]_t$, and $[A \cdot D]_t$ are the number densities of acceptor A -beads, donor D -beads, and associated bodies $A \cdot D$ at time t , respectively. At equilibrium state, the $[A]_t$, $[D]_t$, and $[A \cdot D]_t$ maintain invariable, and thus $d[A]_t/dt = d[A \cdot D]_t/dt = 0$. The equilibrium constant K_{eq} is the ratio of k_a to k_d ,

$$K_{eq} = \frac{k_a}{k_d} = \frac{[A \cdot D]_e}{[A]_e \cdot [D]_e} \quad (S3)$$

where $[A]_e$, $[D]_e$, and $[A \cdot D]_e$ are respectively the number densities of A , D , and $A \cdot D$ at equilibrium state. From Eqs. S1 and S2, we arrive at the relationship

$$\frac{d[A]_t}{dt} + \frac{d[A \cdot D]_t}{dt} = 0 \quad (S4)$$

and thus $[A]_t + [A \cdot D]_t$ is unchanged. Its value is equal to the initial density of A -beads, $[A]_0$

$$[A]_t + [A \cdot D]_t = [A]_0, \text{ at any time} \quad (S5)$$

Substituting Eqs. S3 and S5 into Eq.S1, and considering $[A]_t = [D]_t$ for the equimolar reaction, we can deduce the formula

$$\frac{d[A]_t}{dt} = -k_d \cdot K_{eq}[A]_t^2 + k_d([A]_0 - [A]_t) \quad (S6)$$

The solution of differential equation is given by

$$\ln \left\{ \frac{[A]_t - [A]_2}{[A]_t - [A]_1} \right\} = ([A]_1 - [A]_2)k_d \cdot K_{eq}t + \ln \left\{ \frac{[A]_0 - [A]_2}{[A]_0 - [A]_1} \right\} \quad (S7)$$

$$[A]_1 = -0.5 \left\{ 1 / K_{eq} + (1 / K_{eq}^2 + 4[A]_0 / K_{eq})^{1/2} \right\} \quad (S8)$$

$$[A]_2 = -0.5 \left\{ 1 / K_{eq} - (1 / K_{eq}^2 + 4[A]_0 / K_{eq})^{1/2} \right\} \quad (S9)$$

Herein, $[A]_1$ and $[A]_2$ are variable depending on the K_{eq} and $[A]_0$ (calculated by Eqs. S3 and S5). Thereby, the value of $\ln\{([A]_t - [A]_2)/([A]_t - [A]_1)\}$ is a linear function of time t , and the slope is equal to the value of $([A]_1 - [A]_2)k_d \cdot K_{eq}$.

5. Equilibrium constant at various polymer concentrations

For the systems at polymer concentrations of $\phi=0.10$, $\phi=0.20$, and $\phi=0.30$, we also calculated the equilibrium constant K_{eq} according to the equation of $K_{eq} = [A \cdot D]_e / ([A]_e \cdot [D]_e)$ (see Eq. S3 of ESI), where the $[A \cdot D]_e$, $[A]_e$, and $[D]_e$ are the number densities of associated body ($A \cdot D$), acceptor (A), and donor (D) at equilibrium state, respectively. The amounts of associated body ($N_{A \cdot D, e}$), acceptor ($N_{A, e}$), and donor ($N_{D, e}$) at the equilibrium state of simulations are used to calculate the $[A \cdot D]_e$, $[A]_e$, and $[D]_e$, respectively. Table S1 shows the values of $N_{A \cdot D, e}$, $N_{A, e}$, $N_{D, e}$, and K_{eq} for various polymer concentrations ϕ . The K_{eq} is $262.74 r_c^3$, $274.37 r_c^3$, $259.61 r_c^3$, and $270.76 r_c^3$ for $\phi = 0.10$, $\phi=0.20$, $\phi=0.30$, and $\phi=0.40$, respectively. Therefore, as ϕ changes, the K_{eq} maintains an approximate value around $266.87 r_c^3$.

Table S1. The amounts of acceptor ($N_{A, e}$), donor ($N_{D, e}$), and associated body ($N_{A \cdot D, e}$) of the hydrogen bonds, as well as the K_{eq} in the gel systems with various polymer concentrations.

	$N_{A, e}$	$N_{D, e}$	$N_{A \cdot D, e}$	K_{eq}/r_c^3
$\phi = 0.10$	74±1	74±1	54±1	262.74±13.88
$\phi = 0.20$	117±2	117±2	139±2	274.37±14.55
$\phi = 0.30$	155±4	155±4	231±4	259.61±19.87
$\phi = 0.40$	182±6	182±6	332±6	270.76±24.53

6. Dissipated energy in the loading-unloading tests

We carried out the simulations of loading-unloading tests for the ABC copolymer gels under various polymer concentrations ϕ , force constants k_A , and cutoff angles θ_c of AHD potential (see Eq. 2 of main text). The gels were stretched to a given strain $\varepsilon_{\text{load}}$ with tensile rate $0.2\tau^{-1}$, and then the tensile force was switched off. Mechanical hysteresis is presented in all the samples, and the dissipated energy U_{hys} is defined as the area of the mechanical hysteresis loop. Figure S4 shows the U_{hys} as a function of given strain $\varepsilon_{\text{load}}$ for ABC graft copolymer gels with various ϕ , k_A , and θ_c . It can be seen that the U_{hys} is enhanced with increasing ϕ , k_A , or decreasing θ_c .

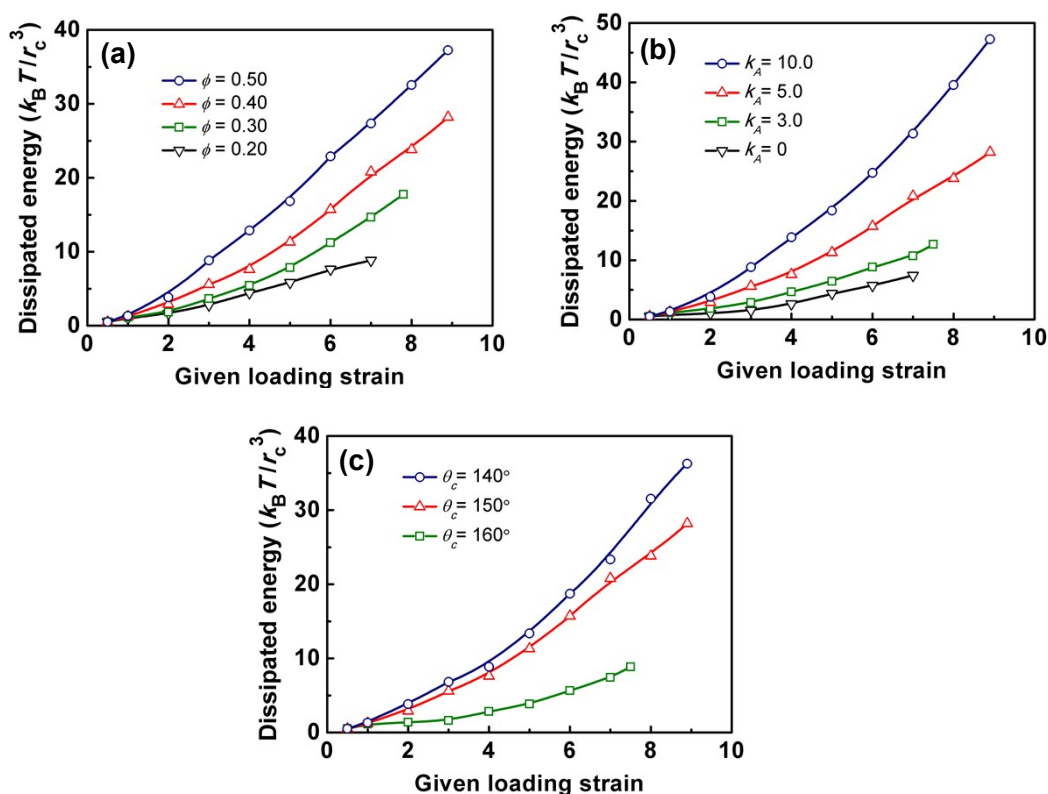


Figure S4. Dissipated energy as a function of given strain in the loading-unloading tests for ABC graft copolymer systems under various (a) polymer concentrations ϕ , (b) force constants k_A and (c) cutoff angles θ_c of the AHD potential.

7. Evolution of energy of hydrogen bond in the cycle tests

We then implemented the elongation-compression cycle tests for the ABC graft copolymer gel with $\phi = 0.40$. The gel is under compression with a rate of $-0.2 \tau^{-1}$ in the cycle tests. The evolution of the energy of hydrogen bonds in the cycle tests is examined. Figure S5 shows the relationship between the hydrogen bond energy and the strain in the compression processes of the first three cycles. It can be seen that the hydrogen bond energy rises around $\varepsilon=1.0$, which causes the bump around $\varepsilon=1.0$ in the unloading curves (see Figure 6c of the main text).

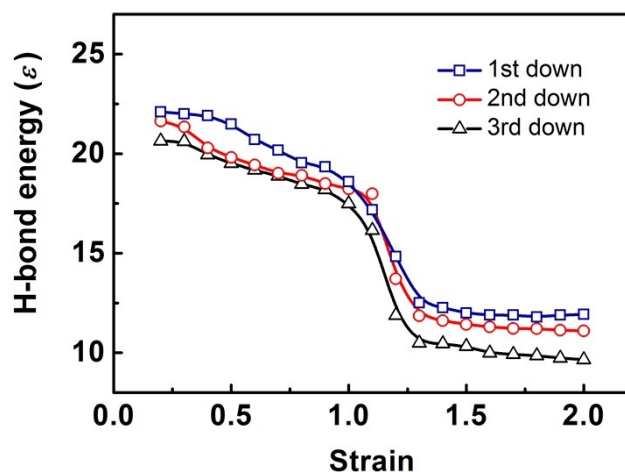


Figure S5. Hydrogen bond energy as a function of strain in the compression processes of the first three cycles of elongation-compression tests for the ABC copolymer gels with $\phi = 0.40$.